UDC 624.012

COMPARATIVE STUDY ON BENDING PERFORMANCE NUMERICAL SIMULATION OF DIFFERENT TYPES OF FRP REINFORCED CONCRETE BEAMS BASED ON ANSYS

Liu Qian[1], A. V. Tur[2]

[1] Graduate student, Brest State Technical University, Brest, Belarus, e-mail: tg5682647234@163.com
[2] Candidate of Technical Sciences, Associate Professor, Head the Department of Architecture, Brest State Technical University, Brest, Belarus, e-mail: aturphd@gmail.com

Abstract

By simulating a three-point bending loading process, the failure modes, load-deflection curves, flexural stiffness, ultimate bearing capacity, and crack propagation modes of each model are compared and analyzed. Simulation results show that the reinforced concrete beam model (Steel-RC) exhibits typical elastoplastic behavior, ultimately resulting in ductile failure due to steel bar yielding ($P_u \approx 56{,}0$ kN, $\delta_u \approx 40{,}0$ mm). All FRP-reinforced beam models adopted an over-reinforced design, and the final failure mode was the crushing of the concrete in the compression zone, exhibiting brittle failure characteristics. The mechanical properties of different FRP reinforcement materials, especially the elastic modulus, play a decisive role in the bending performance of beams: the CFRP reinforced beam model ($E_f = 124{,}2$ GPa) has the highest bending stiffness and ultimate bearing capacity ($P_u \approx 125{,}0$ kN) and the lowest ultimate deflection ($\delta_u \approx 30{,}0$ mm); among all FRP reinforced beams, the GFRP reinforced beam model ($E_f = 45{,}0$ GPa) has the lowest post-cracking stiffness and ultimate bearing capacity ($P_u \approx 82{,}5$ kN), and the largest ultimate deflection ($\Delta u \approx 40{,}0$ mm); the performance of the AFRP reinforced beam model ($E_f = 50{,}1$ GPa) is between the two ($P_u \approx 86{,}4$ kN, $\Delta u \approx 35{,}0$ mm). This study confirms the effectiveness of the finite element method in simulating the stress behavior of FRP-reinforced concrete beams. The results quantify the key differences in flexural properties among different FRP reinforcement materials, providing an important numerical basis and design reference for the engineering community to rationally select FRP materials based on structural performance requirements (strength control or stiffness control) when facing durability challenges.

Keywords: FRP reinforcement, concrete beam, bending performance, numerical simulation, load-deflection curve, SOLID65, William – Warenke.

СРАВНИТЕЛЬНОЕ ИССЛЕДОВАНИЕ ЭФФЕКТИВНОСТИ ИЗГИБА. ЧИСЕЛЬНОЕ МОДЕЛИРОВАНИЕ РАЗЛИЧНЫХ ТИПОВ FRP ЖЕЛЕЗОБЕТОННЫХ БАЛОК НА ОСНОВЕ ANSYS

Лю Цянь, А. В. Тур

Реферат

Чтобы систематически сравнить различия в изгибочных характеристиках различных типов железобетонных балок из волоконно-армированных полимеров (ФРП), в настоящей статье установлены четыре уточненные трехмерные нелинейные цифровые модели с использованием крупномасштабного программного обеспечения конечных элементов общего назначения ANSYS. В этих моделях используются обычные стальные прутки, прутки из полимера, армированного стекловолокном (GFRP), прутки из полимера, армированного арамидным волокном (AFRP), и прутки из полимера, армированного углеродным волокном (CFRP) в качестве основного армирования на растяжение, поддерживая полную консистенцию в геометрических размерах, прочности бетона и соотношении армирования (ρ = 0,56 %). Моделируя трехточечный процесс загрузки изгиба, сравниваются и анализируются режимы сбоя, кривые отклонения нагрузки, жесткость изгиба, конечная несущая способность и режимы распространения трещин каждой модели. Результаты моделирования показывают, что модель железобетонных балок (Steel-RC) демонстрирует типичное эластопластическое поведение, в конечном счете, приводящее к гибкому отказу из-за подачи стальной штанги (Pu ≈ 56,0 kN, δu ≈ 40,0 mm). Все модели железобетонных балок из ФРП приняли конструкцию, чрезмерно армированную, и окончательным режимом отказа было дробление бетона в зоне сжатия, демонстрируя хрупкие характеристики отказа. Механические свойства различных армирующих материалов из ФРП, особенно модуль эластичности, играют решающую роль в производительности изгиба балок: модель железобетонных балок из ХФРП (Ef = 124,2 GPa) имеет самую высокую жесткость изгиба и конечную несущую способность (Pu ≈ 125,0 kN); среди всех усиленных балков из FRP модель усиленного балка из GFRP (Ef = 45,0 GPa) имеет самую низкую посттрещиновую жесткость и конечную несущую способность (Pu ≈ 82,5 kN), а также наибольшее конечное отклонение (Δu ≈ 40,0 mm); производительность модели усиленного луча AFRP (Ef = 50,1 GPa) находится между двумя (Pu ≈ 86,4 kN, Δu ≈ 35,0 mm). Это исследование подтверждает эффективность метода конечных элементов в моделировании напряженного поведения FRP-армированных бетонных балок. Результаты количественно определяют ключевые различия в свойствах изгиба между различными армирующими материалами из ФРП, обеспечивая важную цифровую основу и конструкционную ссылку для инженерного сообщества для рационального выбора материалов из ФРП на основе требований к структурным характеристикам (контроль прочности или контроль жесткости) при столкновении с проблемами долговечности.

Ключевые слова: армировка FRP, бетонная балка, производительность изгиба, цифровое моделирование, кривая отклонения нагрузки, SOLID65, Уильям – Варенке.

1 Introduction

1.1 Durability Challenges of Reinforced Concrete Structures

Reinforced concrete (RC) structures, with their excellent load-bearing capacity, good integrity, and economy, have been the most widely used structural form in global civil engineering for over a century. However, as many infrastructure projects enter their mid-to-late service stages, the durability issues of traditional reinforced concrete structures have become increasingly prominent, posing a key bottleneck to structural safety and service life. Under corrosive conditions such as marine environments, deicing salt environments in cold regions, and industrial pollution, the intrusion of chloride ions (Cl^-) or carbonization of concrete can damage the passivation film on the surface of the reinforcing steel, inducing corrosion.

Reinforcing steel corrosion is an electrochemical process, and its products (rust) can expand to 2 to 6 times the volume of the original reinforcing steel. This expansion stress causes the concrete cover to crack and peel off, further accelerating the intrusion of corrosive media, creating a vicious cycle. Reinforcing steel corrosion not only directly reduces the effective cross-sectional area of the reinforcing steel and deteriorates its mechanical properties, but also severely weakens the bond between the steel and concrete, ultimately leading to a significant decrease

in the structural load-bearing capacity and even brittle failure. Statistics show that the economic losses caused by steel corrosion in structural repair, reinforcement, and replacement are enormous, posing a serious challenge to social resources and environmental sustainability (Yashin, 2025). Therefore, finding alternative materials that can fundamentally solve the corrosion problem has become a research hotspot and urgent need in the field of structural engineering.

1.2 FRP Reinforcement as a High-Performance Alternative

To address the durability shortcomings of traditional steel reinforcement, fiber-reinforced polymer (FRP) composites, possessing both high strength and excellent corrosion resistance, have emerged (Li et al., 2025). FRP reinforcement is typically composed of high-performance fibers (such as glass fiber, carbon fiber, and aramid fiber) combined with a resin matrix, offering a range of advantages including lightweight, high strength, corrosion resistance, fatigue resistance, and electromagnetic insulation (Li et al., 2025).

The most prominent advantage of FRP reinforcement lies in its chemical inertness. In harsh chemical environments such as chloride salts, acids, and alkalis, FRP materials exhibit extremely strong resistance and do not undergo electrochemical corrosion similar to that of steel reinforcement (Zhao et al., 2025). This characteristic makes it an ideal alternative to steel reinforcement and a solution to corrosion problems, particularly suitable for offshore platforms, cross-sea bridges, chemical plants, and cold-region infrastructure exposed to de-icing salts (Sbahieh et al., 2022).

Furthermore, the application of FRP demonstrates significant economic and environmental benefits throughout the entire life cycle of the structure. Although the initial procurement cost of FRP reinforcement is higher than that of ordinary steel bars, numerous studies have shown that FRP structures can significantly reduce the frequency of inspection, maintenance, and reinforcement during the service life of a structure (Sbahieh et al., 2023). A life-cycle cost (LCC) and life-cycle assessment (LCA) analysis of a large GFRP-RC flood control channel in Saudi Arabia shows that the GFRP-RC solution has significant economic and environmental advantages over a 100-year design life compared to epoxy-coated steel reinforcement (ECS). This combined benefit of an ultra-long service life and extremely low maintenance requirements makes FRP an important approach to achieving sustainable infrastructure construction.

1.3 Differences in Mechanical Properties and Serviceability Challenges

Although FRP (Fiber Reinforced Plastic) offers significant advantages in durability, its mechanical behavior differs fundamentally from that of traditional steel reinforcement. Therefore, in structural design, FRP bars cannot be simply considered a one-to-one replacement for steel reinforcement. In particular, the difference in their stress-strain constitutive relations directly determines the structural performance and failure mode of the member.

Firstly, regarding ductility and brittleness, ordinary steel reinforcement (such as HRB400) exhibits typical elastoplastic behavior: once the stress reaches the yield strength, it enters a relatively obvious yield plateau stage, allowing the member to undergo significant plastic deformation and absorb a large amount of deformation energy. This ductile failure is usually accompanied by large deflection and wide cracks, providing a clear visual warning of impending structural failure. In stark contrast, various types of FRP bars exhibit essentially a linear elastic response throughout the entire process from tension to failure, possessing almost no plastic deformation capacity. Once the tensile stress reaches its ultimate tensile strength, the reinforcing bar will suddenly fracture, exhibiting typical brittle failure with insufficient deformation warning signs (Barris et al., 2012).

Secondly, in terms of elastic modulus (stiffness), E is a key parameter controlling the stiffness level of a member after cracking. Based on the material parameters used in this study (see Table 2), the elastic modulus E_s of HRB400 steel reinforcement is approximately 206,0 GPa. The elastic modulus of FRP reinforcement varies considerably: the elastic modulus of CFRP reinforcement is$E_f \approx 124,2$ GPa, relatively close to that of steel reinforcement; while the elastic moduli of AFRP reinforcement ($E_f \approx 50,1$ GPa) and GFRP reinforcement ($E_f \approx 45,0$ GPa) are significantly lower, only about 22 %–24 % of that of steel reinforcement.

Because FRP, especially GFRP and AFRP, exhibits both low elastic modulus and linear elastic brittle failure characteristics, FRP-RC components face two core challenges in design and service performance control.

The first is the control of the serviceability limit state (SLS). Due to the greater strain produced by low-modulus FRP under the same tensile force, the overall stiffness of the component decreases significantly after concrete cracking. This leads to FRP-RC beams often exhibiting greater deflection and wider cracks under service loads, making them more susceptible to service performance limitations compared to reinforced concrete beams (Renić & Kišiček, 2021). In these components, the controlling conditions are often primarily governed by the serviceability limit state (e.g., deflection and crack width) rather than the ultimate limit capacity (ULS) (Su et al., 2025).

The second is the control of ductility and failure mode under the ultimate limit state (ULS). Given that FRP bars exhibit extreme brittleness and instantaneous tensile failure, existing design codes (such as ACI 440.1R-15) generally recommend an over-reinforced design approach, where the FRP reinforcement ratio ρ_f is greater than the equilibrium reinforcement ratioρ_{fb} ($\rho_f > \rho_{fb}$). This ensures that when the member reaches its ultimate limit state, concrete crushing in the compression zone occurs preferentially, rather than the initial tensile failure of the FRP bars (Barris et al., 2012). Although concrete crushing itself is still brittle failure, its development process is relatively more gradual, usually accompanied by more pronounced crack evolution and increased deflection. Compared to the sudden fracture of FRP bars, it can provide a more perceptible early warning of structural failure to some extent.

Insummary, the differences in constitutive relations and stiffness characteristics of FRP reinforcement not only alter the failure mechanism of the component, but also require FRP-RC structures to simultaneously consider the dual control requirements of the serviceability limit state and the ultimate bearing state during design.

1.4 Research Objectives and Innovations

In recent years, numerous experimental (Deng et al., 2009; Sakar & Celik, 2025) and numerical (Said et al., 2021) studies have investigated FRP-reinforced and FRP-strengthened beams, including prestressed FRP strengthening of existing RC beams.However, as this study points out, systematic and benchmark-comparative numerical simulations of different types of FRP reinforcement (especially GFRP, AFRP, and CFRP) with traditional steel reinforcement under identical geometric dimensions, concrete strength, and reinforcement ratios still require further development (Sbahieh et al., 2022).

Therefore, the core objective of this study is to establish four sets of numerical models of concrete beams (Steel-RC, GFRP-RC, AFRP-RC, CFRP-RC) with identical parameters except for the tensile reinforcement material, using a validated nonlinear finite element (FEA) framework, and to perform detailed simulations and comparative analyses of their entire stress process under three-point bending loads.

The innovation of this study lies in the fact that, by strictly controlling variables (geometry, concrete, reinforcement ratio $\rho = 0,56$ %), this simulation study was able to "isolate" and "quantify" the direct impact of the constitutive properties of tension reinforcement (i. e., elastic modulus, strength, and ductility) on the overall flexural performance of concrete beams (including stiffness, bearing capacity, deflection, and failure mode). The significance of this study is that its simulation results provide designers with an intuitive and quantitative performance benchmark, clearly revealing the design trade-offs faced when selecting different FRP reinforcement materials (e. g., the durability gains of GFRP versus SLS penalty, the strength gains of CFRP versus brittleness risk), providing direct numerical basis and theoretical support for rational FRP material selection and optimization design in specific engineering projects (such as corrosive environments).

2 Finite Element Modeling Strategy

This study established four sets of three-dimensional nonlinear finite element models based on the large-scale general-purpose finite element analysis software ANSYS platform. The effectiveness of the modeling strategy has been widely verified in the field of civil engineering (Bai et al., 2024).

2.1 Geometric Model and Element Division

To ensure fairness in the comparison, the four beam models (Steel-RC, GFRP-RC, AFRP-RC, CFRP-RC) are geometrically and reinforcement-completely identical: the rectangular cross-section dimensions are $b \times h = 180$ mm × 250 mm, the total length is $L = 2100$ mm, and the calculated span is $L0 = 1800$ mm; the tension zone is reinforced with 2 main bars of diameter ϕ 12 mm, and the compression zone is reinforced with 2 stirrups of diameter ϕ 8 mm; the stirrups are... HPB300, diameter 8 mm, spacing 100 mm; concrete cover thickness 25 mm. The tensile reinforcement ratio of all models is uniformly set at $\rho = 0,56$ %.

https://doi.org/10.36773/1818-1112-2025-138-3-45-52

Concrete was modeled using ANSYS SOLID65 eight-node hexahedral elements, with nodes having three translational degrees of freedom, capable of characterizing plasticity, compressive crushing, and tensile cracking behaviors (Bai et al., 2024). Reinforcing materials (main bars, stirrups, and gussets) were modeled using LINK180 two-node rod elements, which are uniaxial tension/compression elements. These elements also have three translational degrees of freedom and do not bear bending moments, consistent with the characteristic of embedded reinforcement being primarily subjected to axial forces (Halahla, 2018). To avoid stress concentration at the loading zone and supports, which could lead to localized failure, steel pads were installed on both the loading plate and the supports, and the models were simulated using SOLID185 elements.

The overall finite element modeling arrangement is illustrated in Figure 1. The mesh was mapped, with an element size of approximately 25 mm. All four models had the same mesh size, containing 7,680 nodes and 5,518 elements, with the concrete main body (C40) containing 5,950 nodes and 4,536 elements.

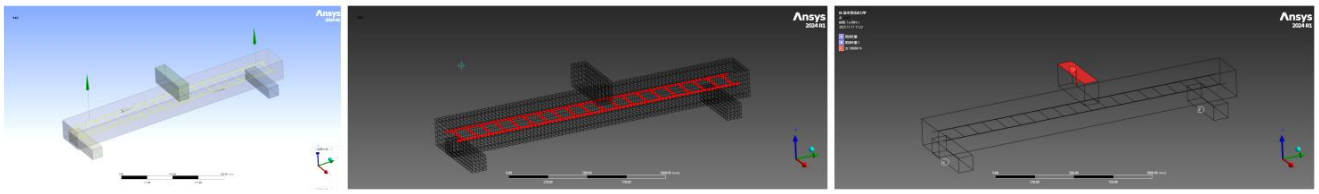

a) overall geometry and loading; b) solid and bar elements with mesh; c) boundary conditions and loading application

Figure 1 – Finite element model of the three-point bending beam

2.2 Material Constitutive Models and Formulas

Material nonlinearity is the core of numerical simulation of concrete structures. This paper adopts a constitutive setting consistent with mechanical mechanisms in ANSYS: concrete is characterized by the built-in SOLID65 model, and its failure criterion is based on the Willam – Warnke five-parameter yield surface; the uniaxial stress-strain rise segment under compression is represented by a Hognestad parabola as $\sigma_c = f_c'[2(\epsilon_c/\epsilon_0) - (\epsilon_c/\epsilon_0)^2]$ (applicable to $\epsilon_c \le \epsilon_0$), where f_c' is the peak compressive stress of concrete (in this paper, f_{ck} = 26,8 MPa), ϵ_c is the compressive strain of concrete, and ϵ_0 is the peak strain; the tensile stage is approximated as linear elastic, taking $\sigma_t = E_c$, ϵ_t and $\epsilon_t \le \epsilon_{cr} = f_{tk}/E_c$ (where E_c is the elastic modulus of concrete, f_{tk} = 2,39, and MPa is the tensile strength). When the principal tensile stress exceeds f_{tk}, the stiffness is corrected at the integration point according to the concept of diffuse cracking. If all principal stresses are compressive stresses and cross the yield surface, crushing is considered to have occurred. The shear transfer at the crack surface adopts the equivalent shear retention model $\tau = \beta, G_c, \gamma$, where τ is the shear stress at the crack surface, G_c is the shear modulus, and γ is the shear strain.β_t = 0,2 is taken for cracking and β_c = 0,9 is taken for closure. The steel reinforcement (HRB400) adopts the bilinear kinematic hardening (BKIN) model. Before yielding, it satisfies $\sigma_s = E_s, \epsilon_s$ and $\epsilon_s \le \epsilon_y = f_y/E_s$. After yielding, it takes $\sigma_s = f_y + E_t(\epsilon_s - \epsilon_y)$, where E_s is the elastic modulus of the steel reinforcement, f_y = 521,2 MPa is the yield strength, ϵ_y is the yield strain, and E_t is the tangent modulus of the hardened section (when E_t = 0, it degenerates into ideal elastic-plasticity). FRP reinforcement (GFRP, AFRP, CFRP) follows linear elastic to brittle fracture characteristics, taking $\sigma_f = E_f, \epsilon_f$ (when $\epsilon_f \le \epsilon_{fu}$), and considering it as fracture and reducing the stress to zero once $\epsilon_f > \epsilon_{fu}$; where σ_f and ϵ_f are the stress and strain of the FRP reinforcement, respectively, E_f is the elastic modulus, and ϵ_{fu} is the ultimate tensile strain. Under unified mesh and boundary conditions, the above constitutive models work synergistically: concrete bears the compressive and pre-cracking tensile stiffness, the reinforcement provides ductility and energy dissipation, and FRP, with its high strength and high modulus, enhances tensile load-bearing capacity and post-cracking stiffness, laying the foundation for reliable simulation of load-bearing capacity and deformation response.

2.3 Material Properties, Bonding, and Boundary Conditions

The key material property parameters used in the model are shown in Tables 1 and 2.

Table 1 – C40 concrete material properties

Parameter	Symbol	Value	Unit
Modulus of elasticity	E_c	32,5	GPa
Poisson's ratio	v_c	0,2	–
Standard value of compressive strength	f_{ck}	26,8	MPa
Standard value of tensile strength	f_{tk}	2,39	MPa

The numerical model assumes perfect bond between the reinforcement and concrete. In ANSYS, this is achieved by having concrete elements (SOLID65) and reinforcement elements (LINK180) share nodes to ensure complete consistency of interface displacements. This means that the node degrees of freedom U_X, U_Y, and U_Z are strictly equal between the reinforcement and concrete, thus eliminating the inconsistency between relative slip at the interface and local displacements within cracks. This approach is equivalent to "embedding" the reinforcement into the concrete skeleton at the mesh level, allowing axial forces, shear forces, and constraint reactions to be directly transmitted to surrounding solid elements through shared nodes. This is suitable for macroscopic-level global response analysis. Its advantages include the stable reproduction of load-deflection curves, ultimate bearing capacity, and dominant failure modes, while avoiding parameter uncertainties and convergence risks associated with explicit bond-slip relationships. However, this simplification neglects the interface shear stress-slip dynamics and detailed mechanisms such as splitting cracking and anchorage degradation around the reinforcement. Therefore, when the research focuses on anchorage length, pull-out strength, or local bond degradation, a more refined interface model is required. Given that this paper focuses on the overall load-bearing and deflection response under mid-span bending control, and does not consider bond failure as the dominant failure mode, the aforementioned "perfect bond" assumption is reasonable within engineering accuracy.

Table 2 – Mechanical properties of reinforcing bars

Reinforcement Bar Types	Diameter (mm)	Young's Modulus (Ef or Es) (GPa)	Yield Strength (fy) (MPa)	Ultimate Tensile Strength (fu) (MPa)	Ultimate Strain (ϵ_{fu}) (%)
HRB400 Reinforcing Bars	12	206,0	521,2	642,0	> 10,0
GFRP Bars	12	45,0	–	910,6	2,02
AFRP Bars	12	50,1	–	1306,2	2,61
CFRP Bars	12	124,2	–	2102,1	1,70

Boundary and loading conditions are consistent with the experimental scenario to ensure comparability. Supports are achieved by applying simply supported constraints to the bottom surface of the end steel plates: one end at Y = 150 mm acts as a hinged support, constraining U_X, U_Y, and U_Z to eliminate rigid body displacement; the other end at Y = 1950 mm acts as a roll support, constraining U_X and U_Z and allowing vertical displacement U_Y, avoiding unnecessary redundant constraints and additional internal forces, and consistent with the end-support configuration in the report and illustrations. The loading employs a three-point bending displacement control scheme: a uniform vertical displacement δis applied to the top node of the loading steel plate (SOLID185) at mid-span Y = 1050 mm, and this displacement is increased through multi-step incremental steps, with each step

size denoted as Δδ. Nonlinear iteration is used within each increment until the residuals satisfy the convergence criterion. Displacement control can continue to track the post-peak path after softening and stiffness degradation occur, avoiding numerical instability near the limit point during force-controlled loading. The reaction force is aggregated through the support constraint nodes to obtain the load P, which is recorded together with the mid-span deflection Δ to form the P–Δ response history. The loading process continues until the model reaches the ultimate bearing capacity P_u, the deflection increases sharply, or the values no longer converge. At this point, the crack distribution, principal tensile stress, strain field in the tension/compression zone, and axial force-strain response of the reinforcement are simultaneously output to verify the triggering order and location of the yield or brittle fracture criteria. To ensure uniform load transfer and reduce stress concentration, both loading and support utilize steel pads to achieve surface contact. The displacements of each node on the loading surface are coupled and constrained to maintain approximate rigid body compression, thereby minimizing local indentation effects and more closely resembling experimental conditions. These modeling details collectively ensure consistent representation of boundaries and loads in terms of geometry, constraints, and force transmission paths, making the numerical results interpretable and comparable across the three dimensions of overall stiffness, peak load capacity, and failure mode.

3 Finite Element Model Validation

Before conducting a systematic comparison between models, it is necessary to first verify whether the finite element modeling framework (SOLID65 + LINK180 + Willam – Warnke model) used in this paper can accurately capture the real stress behavior of FRP-RC beams and Steel-RC beams. To this end, we qualitatively and quantitatively compare the numerical model's predictions regarding failure modes, stiffness evolution, and load-bearing capacity with authoritative experimental studies published in the past decade (2015–2025) to establish the model's effectiveness and interpretability. The core of the validation lies in the overall shape of the load-deflection curve, the consistency of the limit state parameters, and whether the control failure mechanism matching the material constitutive model is correctly triggered.

3.1 Steel-RC Model Validation

Based on the comparison with the section theory analysis, the integrated results of the Steel-RC numerical model show that the theoretical ultimate load is approximately $P_u \approx 56{,}0\ \mathrm{kN}$, corresponding to an ultimate deflection of approximately $\delta_u \approx 40{,}0\ \mathrm{mm}$. The failure process is characterized by the initial yielding of the tensile reinforcement, followed by crushing of the concrete in the compression zone, exhibiting typical ductile failure. The load-deflection curve obtained from the finite element method shows a clear yield plateau before approaching the ultimate load, a clear elasto-plastic transition, and a significant decrease in stiffness after yielding. This overall pattern is highly consistent with numerous standard test results on three-point bending of reinforced concrete beams (Karabulut, 2025), indicating that the model can accurately reproduce the elasto-plastic response and ductile characteristics of reinforced concrete beams, and maintains reasonable tracking of load-bearing capacity decay and deflection growth in the post-peak stage.

3.2 Validation of the GFRP-RC Model

The comprehensive analysis results of the GFRP-RC model show that the theoretical ultimate load is approximately $P_u \approx 82{,}5\ \mathrm{kN}$, the ultimate deflection is approximately $\delta_u \approx 40{,}0\ \mathrm{mm}$, and the controlling failure mode is concrete crushing. Compared with Steel-RC, the equivalent bending stiffness in the post-cracking stage is significantly reduced. Under the same load level, the deflection of the GFRP-RC beam is significantly greater than that of the steel beam, which is consistent with the low elastic modulus characteristic of GFRP ($E_f = 45{,}0\ \mathrm{GPa}$). Existing experimental studies have repeatedly confirmed that due to the low E_f, deflection control of GFRP-RC beams is particularly critical during the normal service stage (Bakar et al., 2022), and Di et al. (2023) also listed the deflection limit under the service limit state as one of the core design indicators. It is important to emphasize that, under the unified tensile reinforcement ratio of $\rho = 0{,}56\ \%$ in this paper, the GFRP-RC beam is in the "over-reinforced" range. Numerical predictions show concrete crushing as the controlling failure mode rather than FRP tensile failure, consistent with the experimental observations of Di et al. (2023) on over-reinforced GFRP beams. This also explains the engineering logic of prioritizing deflection and crack control in GFRP design.

3.3 CFRP-RC Model Validation

The comprehensive analysis results of the CFRP-RC model show that the theoretical ultimate load is approximately $P_u \approx 125.0\ \mathrm{kN}$, the ultimate deflection is approximately $\delta_u \approx 30.0, \mathrm{mm}$, and the controlling failure mode is concrete crushing. Compared to Steel-RC ($P_u \approx 56.0\ \mathrm{kN}, \delta_u \approx 40.0\ \mathrm{mm}$) and GFRP-RC ($P_u \approx 82.5\ \mathrm{kN}$, $\delta_u \approx 40.0\ \mathrm{mm}$), CFRP-RC exhibits significantly improved load-bearing capacity and significantly reduced deflection, demonstrating the highest equivalent bending stiffness. This is consistent with the high modulus and high strength characteristics of CFRP ($E_f = 124.2\ \mathrm{GPa}$). The mixed reinforcement test conducted by Tran and Nguyen-Thoi (2025) further demonstrates that specimens containing CFRP reinforcement (CFRP-40S) have a significant advantage in ultimate strength compared to pure steel reinforcement specimens (STEEL-40S). It should be noted that the numerically predicted concrete crushing control failure is consistent with the FRP-RC design philosophy advocated by ACI 440.1R-15 (Kim et al., 2011) and CSA S806 (Baghi, 2015), which "forces" the premature failure of the compression zone concrete through an overmixing strategy of $\rho_f > \rho_{fb}$, thereby avoiding the sudden brittle failure caused by FRP tensile fracture (Barris et al., 2012). Numerous experiments and reviews also indicate that the load-bearing capacity predictions of ACI 440.1R-15 agree well with experimental results, although slightly conservative in some cases (Elsheikh et al., 2024), which is inherently consistent with the numerical performance presented in this paper.

3.4 AFRP-RC Model Validation

The comprehensive analysis results of the AFRP-RC model show that the theoretical ultimate load is approximately $P_u \approx 86{,}4\ \mathrm{kN}$, the ultimate deflection is approximately $\delta_u \approx 35{,}0\ \mathrm{mm}$, and the controlling failure is concrete crushing. Considering that the elastic modulus of AFRP is $E_f = 50{,}1\mathrm{GPa}$, slightly higher than that of GFRP ($E_f = 45{,}0\ \mathrm{GPa}$), but significantly lower than that of CFRP ($E_f = 124{,}2\ \mathrm{GPa}$) and steel reinforcement ($E_s = 206{,}0\ \mathrm{GPa}$) (Salem & Issa, 2023), its load-bearing capacity and stiffness are numerically between GFRP-RC and CFRP-RC, while its overall performance is significantly better than that of Steel-RC within the specified range; specifically, $P_u \approx 86{,}4\ \mathrm{kN}$is between $82{,}5\mathrm{kN}$ and $125{,}0\ \mathrm{kN}$, and $\delta_u \approx 35{,}0\ \mathrm{mm}$ is between approximately Between $40{,}0\ \mathrm{mm}$ and approximately $30{,}0\ \mathrm{mm}$, this "middle" position is perfectly consistent with the ranking of material mechanical properties. Although publicly available measured data for AFRP-RC are slightly less than those for GFRP and CFRP, the numerical study by Saadi et al. (2025) and the experimental results by Sammen et al. (2019) both show that its flexural capacity increases monotonically with the reinforcement ratio, and the load-deflection curves agree well with the finite element analysis, thus providing cross-validation for the numerical conclusions of this paper.

In summary, the SOLID65 + LINK180 + Willam – Warnke modeling framework can stably reproduce the typical bending mechanism dominated by different reinforcement constitutive characteristics under unified mesh, material parameters, and boundary settings: Steel-RC exhibits yield-controlled ductile failure, while FRP-RC generally exhibits crushing failure controlled by the compression zone concrete under the unified reinforcement ratio of 0,56 % in this paper; the stiffness evolution is monotonically ordered with respect to the material modulus, with CFRP having the highest stiffness, followed by AFRP, and then GFRP, while Steel-RC, as a control, shows significant characteristics of elastic-plastic transition and yield plateau; the relative relationship between ultimate bearing capacity and deflection is consistent with recent authoritative tests and standards (ACI 440.1R-15) (Said et al., 2021). From the shape of the load-deflection curve, peak parameters to the triggering of the failure mechanism, the consistency between numerical and experimental data shows that the framework has a good ability to explain and extrapolate the mechanical response of four types of beams, laying a solid foundation for subsequent systematic parameterized comparison and mechanism analysis among the four models.

4 Comparative Analysis of Bending Performance

Based on the completed model verification, this chapter systematically compares the simulation results of four beams with different reinforcement configurations. It focuses on examining their failure process, load-deflection response, bearing capacity, and deformation characteristics. Under unified boundary, mesh, and material settings, the systematic influence of reinforcement mechanical properties on overall bending performance is discussed.

https://doi.org/10.36773/1818-1112-2025-138-3-45-52

4.1 Failure Mode and Crack Development

Based on ANSYS post-processing results, the stress redistribution, crack initiation and propagation, and final failure mode of each model throughout the loading process can be clearly tracked. For a Steel-RC beam, the initial loading stage exhibits a linear elastic response. As the load increases, the concrete at the bottom edge of the maximum bending moment zone at mid-span first reaches its tensile strength and produces vertical cracks. Subsequently, the cracks steadily advance upwards along the height and their number increases. When the load approaches the yield level (approximately 0,8 P_u, which is approximately 45,0 kN under the condition $P_u \approx 56{,}0$ kN), the tensile reinforcement stress reaches the yield strength $f_y = 521{,}2$ MPa, and the beam enters the plastic stage. The mid-span deflection accelerates and exhibits significant ductility. Finally, as the deflection continues to increase, the strain of the concrete at the top edge of the compression zone approaches the ultimate compressive strain, resulting in crushing. The numerical calculation terminates due to stiffness degradation. For the three types of FRP-RC beams (GFRP, AFRP, and CFRP), the overall stress trajectory before cracking is basically the same as that of reinforced concrete beams. After cracking, because the FRP reinforcement remains linearly elastic throughout, the decrease in member stiffness is more significant, especially in low-modulus systems. As the load increases, cracks continue to develop near the mid-span and extend upwards. Under the unified tensile reinforcement ratio of $\rho = 0{,}56$ % set in this paper, all three types of FRP beams are designed according to the over-reinforcement concept ($\rho_f > \rho_{fb}$). Therefore, at failure, the FRP reinforcement has not reached the ultimate tensile strain (i. e., $\epsilon_f < \epsilon_{fu}$), and ultimately all of them are crushed due to the concrete in the compression zone reaching the ultimate compressive strain. During the failure process, there is no plateau similar to the yielding of the reinforcement, exhibiting typical characteristics of linear elastic to brittle failure.

The difference in crack distribution directly reflects the influence of the elastic modulus of the reinforcement on the control of flexural cracks. Figure 2 shows a comparison of crack morphologies under the same load level $P = 80, \mathrm{kN}$, revealing that the FRP beam is in the service-limit transition phase, while the load for the Steel-RC beam is slightly above its theoretical limit, but still usable for morphological comparison of crack modes. The GFRP-RC beam, due to its lowest elastic modulus ($E_f = 45{,}0$ GPa), exhibits greater reinforcement elongation under the same tensile force, resulting in the highest crack height and relatively sparse distribution, leading to a larger individual crack width. The CFRP-RC beam, with its highest elastic modulus ($E_f = 124{,}2$ GPa), has the strongest inhibitory effect on crack propagation, resulting in denser cracks with lower heights, and its morphology is closest to that of a reinforced beam ($E_s = 206{,}0$ GPa). The crack height, density, and width of the AFRP-RC beam fall between the two ($E_f = 50{,}1$ GPa). This pattern of "lower modulus, wider cracks" is consistent with existing experimental research (Bakar et al., 2022) and also aligns with the mechanical nature of FRP, which bears all tensile internal forces without yielding after cracking. The stress contours of the main tensile reinforcement at ultimate load, shown in Figure 3, further confirm that only the Steel-RC beam reaches yielding, whereas all FRP-RC beams remain in the elastic range at failure.

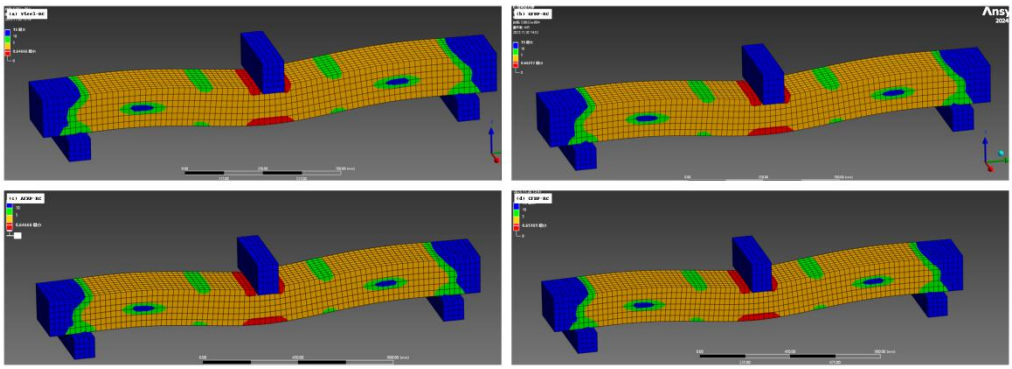

a) Steel-RC; b) GFRP-RC; c) AFRP-RC; d) CFRP-RC

Figure 2 – Comparison of failure patterns at ultimate load

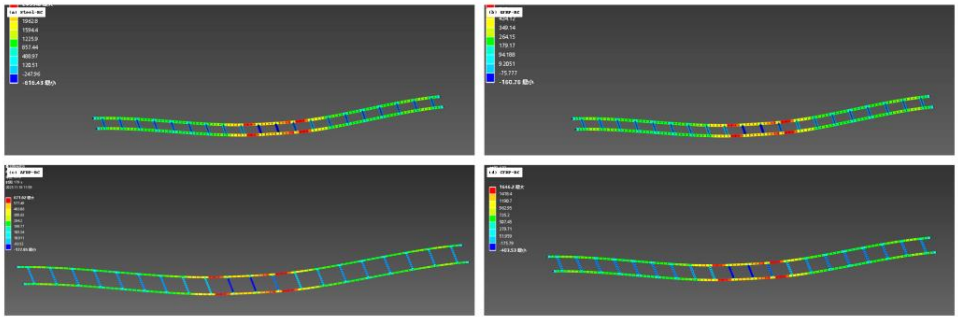

a) Steel-RC; b) GFRP-RC; c) AFRP-RC; d) CFRP-RC

Figure 3 – Stress distribution in main tensile reinforcement at ultimate load

4.2 Load-Deflection Response

The load-deflection curve comprehensively reflects the evolution of stiffness, load-carrying capacity, ductility, and failure mode of a member from the linear elastic stage through the ultimate stage to the post-peak stage. Figure 4 displays the complete responses of the four models, using the ultimate values obtained from the comprehensive theoretical analysis in Chapter 3 as reference points: Steel-RC beam $P_u \approx 56{,}0$ kN, GFRP-RC beam $P_u \approx 82{,}5$ kN, AFRP-RC beam $P_u \approx 86{,}4$ kN, CFRP-RC beam $P_u \approx 125{,}0$ kN. During the pre-cracking stage (Phase I), the curves largely overlap with a load threshold of approximately $P < 25$ kN. At this stage, the cross-section remains uncracked, and the overall flexural stiffness is primarily governed by the uncracked cross-section's moment of inertia $E_c I_g$. The reinforcement type and E_f or E_s exert limited influence on the initial slope. Upon entering the post-cracking stage (Phase II), the contribution from the tensile concrete zone disappears, and tensile internal forces are entirely borne by the reinforcement. The equivalent stiffness is then dominated by the equivalent moment of inertia of the cracked section $E_c I_{cr}$ and the elastic modulus of the reinforcement: CFRP-RC exhibits the steepest curve slope, reflecting the highest post-cracking stiffness $E_f = 124{,}2$ GPa with fully linear elastic behavior approaching the limit state);

Steel-RC shows a high initial slope after cracking (E_s = 206,0 GPa), but the tangent stiffness decreases significantly as the tensile steel approaches yield; AFRP-RC exhibits lower stiffness than the former two (E_f = 50,1 GPa), while GFRP-RC has the lowest stiffness (E_f = 45,0 GPa) with the flattest curve, indicating the weakest deformation resistance. Upon entering the ductility and failure stage (Phase III), Steel-RC exhibits a distinct inflection point at approximately 0,8 $P_u \approx$ 45,0 kN, forming a clear "yield plateau." After significant ductile deformation, it reaches $P_u \approx$ 56,0 kN and gradually transitions to crushing failure. In contrast, the three FRP-RC curves exhibit near-linear growth after cracking until reaching their respective ultimate loads ($P_u \approx$ 82,5 kN,86,4 kN and 125,0 kN), followed by rapid instability due to concrete crushing in the compression zone. They lack a buffer zone for yield warning, exhibiting a "linear elastic to brittle" characteristic. Overall, pre-cracking stiffness is determined by $E_c I_g$, while post-cracking stiffness correlates closely with the relative magnitude of E_f or E_s. CFRP achieves maximum load-carrying capacity and minimum deflection through its high E_f and high strength. Steel-RC demonstrates superior toughness through its ductile plateau region, while AFRP and GFRP rank in the mid-to-low range for stiffness and deflection control based on their E_f values. This sequence aligns with the ultimate load and deformation criteria established in Chapter 3 and corroborates empirical insights from codes and experiments regarding the flexural performance of FRP-RC composites.

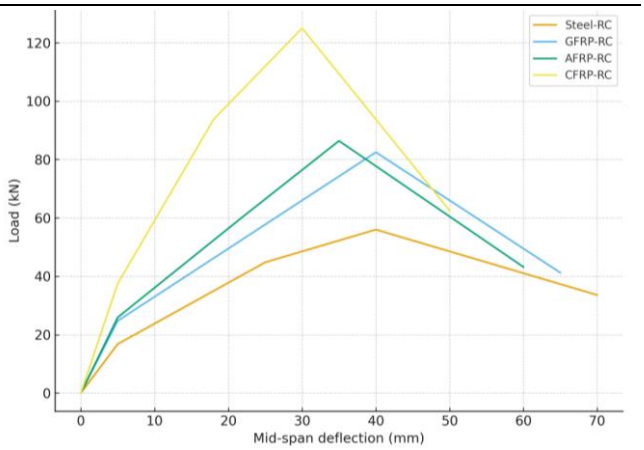

Figure 4 – Load-deflection curve

4.3 Bending Capacity and Deformation Capacity

To accurately and quantitatively compare the performance of each model, Table 3 summarizes the key performance indicators of each model.

Table 3 – Comparison of key performance indicators of each model

Model Number	Cracking Load (kN)	Ultimate Load (Pu) (kN)	Relative Load-Carrying Capacity of Reinforced Concrete Beams	Ultimate Deflection (δu) (mm)	Relative Deflection of Reinforced Beam	Destructive Mode
Steel-RC	25,5	56,0	Reference Benchmark	40,0	Reference Benchmark	Concrete crushing after steel reinforcement yielding
GFRP-RC	24,1	82,5	+47,3 %	40,0	+0,0 %	Concrete crushing
AFRP-RC	24,8	86,4	+54,3 %	35,0	−12,5 %	Concrete crushing
CFRP-RC	26,4	125,0	+123,2 %	30,0	−25,0 %	Concrete crushing

Under the same reinforcement ratio, the ultimate bearing capacities of the four types of beams, based on section theory, are as follows: Steel-RC beam $P_u \approx 56{,}0$ kN, GFRP-RC beam $P_u \approx 82{,}5$ kN, AFRP-RC beam $P_u \approx 86{,}4$ kN, and CFRP-RC beam $P_u \approx 125{,}0$ kN. Compared to reinforced beams, the ultimate bearing capacities of the three types of FRP beams are increased by approximately $47{,}3$ %, $54{,}3$ %, and $123{,}2$ %, respectively. Within the FRP category, CFRP-RC beams have the highest relative bearing capacities, followed by GFRP-RC beams, with AFRP-RC beams in the middle. This result indicates that, under the design premise of over-reinforcement and concrete crushing as the control for failure, the key to flexural bearing capacity lies not only in the strength of the reinforcement but also in its elastic modulus. To achieve the ultimate compressive strain ϵ_{cu} in the compression zone, the neutral axis needs to shift upwards, and the strain ϵ_f in the tension zone is determined by strain compatibility. Therefore, the reinforcement stress $f_f = E_f, \epsilon_f$ is derived from linear elasticity. The larger the value, the better it can counteract the resultant force in the compression zone during internal force equilibrium, thereby increasing the ultimate bending moment and ultimate load. Since $E_f = 124{,}2$ GPa, the f_f corresponding to concrete crushing in CFRP is much higher than that of AFRP ($E_f = 50{,}1$ GPa and GFRP ($E_f = 45{,}0$ GPa), thus achieving the highest bearing capacity among the three types of FRP.

Deformation capacity is directly related to stiffness. Based on theoretical skeleton curves, the mid-span ultimate deflection of the three types of FRP beams is generally on the same order of magnitude as that of reinforced steel beams. Among them, the ultimate deflection of GFRP-RC beams is the largest ($\delta_u \approx 40{,}0$ mm), close to that of Steel-RC beams ($\delta_u \approx 40{,}0$ mm), but significantly greater than that of AFRP-RC beams ($\delta_u \approx 35{,}0$ mm) and CFRP-RC beams ($\delta_u \approx 30{,}0$ mm). CFRP-RC beams have the highest stiffness and the smallest ultimate deflection after cracking, approximately 25 % smaller than that of reinforced steel beams; the deformation capacity of AFRP-RC beams falls between that of GFRP and CFRP. Combining the comparison of cracks and deflections under the same load level (e. g., $P = 80$ kN) in Section 4.1, it can be concluded that under the serviceability limit state, the GFRP-RC beam exhibits the most unfavorable deflection and crack control, while the CFRP-RC beam performs best. This ranking is consistent with the relative magnitude of E_f and agrees with the patterns revealed in experimental literature.

4.4 Ductility and Serviceability Limit State (SLS) Assessment

Regarding ductility, Steel-RC beams exhibit a significant plastic plateau in the range approaching and exceeding $P_u \approx 56{,}0$ kN, demonstrating good toughness through continuous plastic deformation and energy dissipation and deformation redistribution. In contrast, FRP beams, due to the linear elasticity of the tension reinforcement throughout and the absence of a yield stage, show an approximately linear increase in the load-deflection relationship after cracking, rapidly transitioning to instability upon reaching the limit, lacking a clear ductile "buffer zone," and generally exhibiting brittle failure characteristics (Alkhraisha et al., 2020). It is important to emphasize that under the unified oversizing design in this paper, all three types of FRP beams use concrete crushing rather than reinforcement breakage as the control failure mechanism. This mechanism offers stronger predictability than direct FRP fracture, but its essence remains brittle failure, with significantly weaker ductility reserves than reinforced beams.

The serviceability limit state (SLS) primarily focuses on deflection and crack width. The results in Figure 2 and Table 3 show that, under the same service load level, the GFRP-RC beam exhibits the highest deflection and crack width due to its lowest post-cracking equivalent stiffness; the CFRP-RC beam achieves the lowest deflection and crack width due to its highest post-cracking stiffness; the AFRP-RC beam falls in between. This conclusion is consistent with ACI 440.1R-15 and numerous experimental studies (Tran et al., 2025), namely that the design of low-modulus FRP beams is more easily controlled by the Serviceability Limit State (SLS) than by the Serviceability Limit State (ULS), thus requiring priority verification of service performance in engineering design.

The above numerical patterns can be explained using the theoretical framework of ACI 440.1R-15. For an over-reinforced FRP beam controlled by concrete crushing, the FRP reinforcement stress can be given by an analytical formula based on strain compatibility and internal force balance

$$f_f = \left(\sqrt{\frac{(E_f \epsilon_{cu})^2}{4} + \frac{0.85 \beta_1 f_c'}{\rho_f} E_f \epsilon_{cu}} - \frac{E_f \epsilon_{cu}}{2} \right) \leq f_{fu}, \quad (1)$$

where $\rho_f = A_f/(b, d)$ is the reinforcement ratio, E_f is the elastic modulus of FRP, ϵ_{cu} is the ultimate compressive strain of concrete (usually taken as $0{,}003$), f_c' and β_1 are parameters of the concrete compression zone, and f_{fu} is the stress of the FRP reinforcement. Let M_n be the ultimate tensile strength of the FRP.

https://doi.org/10.36773/1818-1112-2025-138-3-45-52

The ultimate bending moment can be approximated as

$$M_n \approx A_f f_f \left(d - \frac{\beta_1 c}{2}\right), \quad (2)$$

where A_f is the area of the FRP under tension, d is the effective height from the resultant point of the tensile reinforcement (or FRP) to the compression edge, and c is the depth of the neutral axis. From the above relationship, it is clear that when the geometric and material parameters such as ρ_f, f_c', and ϵ_{cu} remain consistent, f_f increases with E_f, thereby driving the increase of M_n and P_u; when E_f is low, f_f and M_n decrease accordingly. The numerical ranking obtained in this paper – CFRP-RC beams have the highest load-bearing capacity, followed by AFRP-RC beams, and GFRP-RC beams have the lowest – and the ultimate load-bearing capacity of the three types of FRP-RC beams is significantly higher than that of Steel-RC beams overall – is completely consistent with the theoretical mechanism. This also verifies, from another perspective, the one-to-one correspondence between the ranking of stiffness and service performance after cracking and E_f, thus providing a coherent and interpretable chain of evidence for the design of FRP-RC beams at both the ULS and SLS levels.

Discussion and Significance of the Research

This study, under strict control of geometry, concrete strength, load, and boundary conditions, only varied the type of tensile reinforcement and its constitutive properties. A nonlinear finite element simulation system was used to quantify the differences in flexural performance of four types of beams – steel, GFRP, AFRP and CFRP – under the same reinforcement ratio. The numerical results are consistent with existing experimental and theoretical studies (Bakar et al., 2022) and clearly demonstrate that, under conditions of over-reinforcement and concrete crushing as the control for failure, the key factors determining post-cracking stiffness, crack width, ultimate deflection, and ultimate bearing capacity are not solely tensile strength, but essentially depend on the elastic modulus E_f. Under the unified reinforcement ratio and concrete parameters in this paper, the ranking of ultimate bearing capacity is highly consistent with E_f: CFRP-RC beams have the highest $P_u \approx 125{,}0 \approx 124{,}2$ GPa, followed by AFRP-RC beams with $E_f = 50{,}1$ GPa ($P_u \approx 86{,}4$ kN), and GFRP-RC beams rank last with $E_f = 45{,}0$ GPa ($P_u \approx 82{,}5$ kN), although their $f_u \approx 910{,}6$ MPa is still much higher than the yield strength of the steel reinforcement $f_y \approx 521{,}2$, MPa. Meanwhile, the ultimate bearing capacity of the three types of FRP-RC beams is significantly higher than that of Steel-RC beams ($P_u \approx 56{,}0$ kN), indicating that under the over-stressing strategy to avoid brittle fracture of the reinforcement, FRP beams can outperform traditional reinforced beams at the ultimate state level.

The mechanical reason for this is that when failure is controlled by concrete crushing rather than FRP tensile fracture, the effective internal force in the tension zone is provided by the stress that the reinforcement can develop under a given strain. Based on strain compatibility and internal force balance, it can be deduced that under the condition of fixed ρ_f and concrete parameters, a higher E_f can generate greater tensile force before the compression zone reaches the ultimate compressive strain ϵ_{cu}, making it easier to achieve balance with the resultant force in the compression zone, thus increasing the ultimate bending moment and ultimate load P_u of the section. Conversely, when E_f is low (such as in GFRP), the stress and strain energy of the tensile reinforcement has not been fully utilized when the compression zone approaches ϵ_{cu}, resulting in suppressed section efficiency and bearing capacity. The resulting "modulus-driven" bending enhancement mechanism is consistent with the theoretical framework of ACI 440.1R-15, indicating that under the same reinforcement and concrete conditions, P_u increases monotonically with E_f, and is not solely dependent on the level of f_u.

These conclusions provide a clear basis for trade-offs in engineering material selection and construction. When the primary design objective is to address corrosion and deflection control requirements are relatively lenient or allow for a moderate increase in cross-section, GFRP offers good cost-effectiveness. However, the reduced stiffness after cracking due to lower E_f must be fully recognized: greater deflection and crack width under the same service load, making the design more susceptible to SLS rather than ULS control (Tran et al., 2025). If high load-bearing capacity and high stiffness are required while maintaining corrosion resistance (e. g., for large spans, heavy loads, or deformation-sensitive members), CFRP is a better choice: at the same reinforcement ratio, its P_u is approximately twice that of a reinforced beam, and the ultimate deflection is reduced by about a quarter. However, it requires higher material costs and strict adherence to over-reinforcement principles (e. g., ensuring $\rho_f > \rho_{fb}$) to achieve predictable concrete crushing failure rather than sudden reinforcement breakage. For a performance-cost trade-off, AFRP provides an intermediate solution: load-bearing capacity and stiffness fall between GFRP and CFRP and are generally superior to Steel-RC, but require comprehensive evaluation considering environmental sensitivity and life-cycle costs. It is important to emphasize that reinforced beams still possess unique advantages in terms of ductility and failure early warning: their yield plateau and greater plastic rotation capacity can reduce the risk of sudden failure through energy dissipation and deformation redistribution. This is something that current FRP-RC systems cannot completely replace, and design choices must carefully consider this.

Methodologically, the main contribution of this paper lies in constructing a rigorously "consistent benchmark" numerical test field: eliminating external differences in geometry, reinforcement, material strength, load, and boundaries in ANSYS, and only changing the $E_f$and "elastoplastic/linear elastic" properties of the tension reinforcement, thereby clearly and quantitatively separating the pure influence of reinforcement constitutive differences on bending performance within a unified framework. This systematic comparison across materials and indices transcends the limitations of single-item physical tests in terms of specimen size and controllability of operating conditions, enabling parallel and transparent comparison of multi-dimensional indices such as peak load capacity, post-cracking stiffness, crack control, and ultimate deflection. The evidence obtained not only deepens the understanding of the bending mechanism of FRP-RC components, but also provides a reusable basis for optimized design and specification refinement, and lays a solid foundation for subsequent comprehensive numerical-experimental studies that incorporate the coupling effects of long-term loads, fatigue and environment.

Conclusion

This paper utilizes the ANSYS finite element platform to systematically compare the flexural responses of four groups of concrete beams using ordinary steel reinforcement (HRB400), GFRP, AFRP, and CFRP, under the premise of completely consistent geometric dimensions, concrete strength, loads, boundary conditions, and reinforcement ratios of 0,56 %. Only the type of tensile reinforcement and constitutive properties were changed. The numerical results are generally consistent with authoritative experimental literature and section theory analysis (Bakar et al., 2022), indicating that the modeling scheme based on SOLID65 (simulating the Williams–Warnke nonlinear behavior of concrete) and LINK180 (simulating reinforcement) can reliably reproduce the key characteristics of beams with different reinforcement in terms of load-deflection evolution, stiffness degradation, and failure mechanisms. Specifically, the Steel-RC beam exhibits ductile failure dominated by tensile reinforcement yielding, while the FRP-RC beam consistently shows brittle failure controlled by concrete crushing. Furthermore, the theoretical ultimate bearing capacity and the finite element results agree well in terms of order of magnitude and relative order of magnitude. Further performance comparisons clearly show that the type of FRP has a significant impact on flexural performance, and the decisive parameter is not only tensile strength, but also the elastic modulus E_f. Under the same reinforcement ratio and over-reinforcement design (with concrete crushing as the control for failure), the flexural stiffness in the post-cracking stage is jointly controlled by "reinforcement modulus + moment of inertia of the cracked section", with the overall ranking as follows: CFRP-RC > Steel-RC > AFRP-RC > GFRP-RC. Regarding ultimate bearing capacity, the ultimate loads obtained based on section theory are: Steel-RC beam $P_u \approx 56{,}0$ kN, GFRP-RC beam $P_u \approx 82{,}5$ kN, AFRP-RC beam $P_u \approx 86{,}4$ kN, and CFRP-RC beam $P_u \approx 125{,}0$ kN. The corresponding performance ranking is: CFRP-RC ($125{,}0$ kN) > AFRP-RC($86{,}4$ kN) > GFRP-RC ($82{,}5$ kN) > Steel-RC ($56{,}0$ kN). Regarding deformation capacity, the estimated mid-span ultimate deflection based on the theoretical skeleton curve is as follows: Steel-RC beam $\delta_u \approx 40{,}0$ mm, GFRP-RC beam $\delta_u \approx 40{,}0$ mm, AFRP-RC beam $\delta_u \approx 35{,}0$ mm, CFRP-RC beam $\delta_u \approx 30{,}0$ mm. The overall order is: GFRP-RC $\approx$ Steel-RC ($\approx 40{,}0$ mm) > AFRP-RC ($35{,}0$ mm) > CFRP-RC ($30{,}0$ mm). Combining deflection and crack distribution under service loads, it can be determined that GFRP-RC beams exhibit the most unfavorable deflection and crack control from the SLS perspective, while CFRP-RC beams perform the best.

The comparison of failure and ductility characteristics further points to clear design implications. Steel-RC beams undergo a stage of steel bar yielding and plastic development before approaching the ultimate load, exhibiting a clear yield plateau and strong energy dissipation capacity. In contrast, GFRP-RC, AFRP-RC, and CFRP-RC beams all experience failure controlled by concrete crushing. Although this provides some warning compared to sudden reinforcement breakage, their overall ductility is significantly lower than that of Steel-RC beams. Therefore, in engineering applications, over-sizing design and reasonable safety reserves are necessary to compensate for the insufficient ductility. Regarding material selection decisions, CFRP, with its higher E_f, can significantly improve load-bearing capacity and stiffness under the same reinforcement ratio: In the case of this study, the ultimate load-bearing capacity of the CFRP-RC beam is approximately 2.2 times that of the Steel-RC beam, and the ultimate deflection is reduced by about one-quarter. It is suitable for components with simultaneously stringent requirements for strength and deformation, but it requires higher material costs and strict adherence to the over-reinforcement principle to ensure the concrete crushing failure mode. Although GFRP can effectively solve the corrosion problem, due to its lowest E_f, the stiffness reduction after cracking is the most significant. Under the same service load, it is more prone to larger deflection and cracks. The design is often constrained by SLS rather than ULS, and the control of deflection and crack limits must be strengthened. AFRP provides a pragmatic trade-off between performance and cost. Its load-bearing capacity and stiffness are between GFRP and CFRP and are generally superior to Steel-RC, making it suitable for scenarios that balance performance and economy. The final engineering selection should comprehensively consider factors such as structural importance, load conditions, environmental erosion level, deformation limits, and life-cycle cost. Based on the specifications, the ULS and SLS should be double-checked to reasonably determine the reinforcement scheme and target performance indicators. In conjunction with key quantitative information such asE_f, P_u, and δ_u, a design path for balanced optimization of durability, load-bearing capacity, and service performance should be formed.

References

1. 13.65. SOLID65 – 3-D Reinforced Concrete Solid / ANSYS Inc. // In ANSYS Mechanical APDL Theory Reference (Release 18.2). – 2017. – Retrieved November, 15.
2. Serviceability and flexural behavior of concrete beams reinforced with basalt fiber-reinforced polymer (BFRP) bars exposed to harsh conditions / H. Alkhraisha, N. Tello, F. Albed, H. Mhanna // Polymers. – 2020. – Vol. 12 (9). – P. 2110. – DOI: 10.3390/polym12092110.
3. Flexural strength of concrete beam reinforced with CFRP bars: A review / M. B. C. Bakar, R. S. M. Rashid, M. Amran [et al.] // Materials. – 2020. – Vol. 15 (3). – P. 1144. – DOI: 10.3390/ ma15031144.
4. Bai, H. Multiscale analysis of the flexural performance of FRP reinforced concrete structures. Canadian Journal of Civil Engineering / H. Bai, X. Yuan, Z. Gong // Advance online publication. – 2024. – DOI: 10.1139/cjce-2024-0005.
5. Baghi, H. Shear strengthening of reinforced concrete beams with SHCC-FRP panels : diss… Doctoral / Baghi Hadi ; Universidade do Minho ; Research Gate, 2015. – 236 l.
6. Serviceability limit state of FRP RC beams / C. Barris, M. Baena, L. Torres, K. Pilakoutas // Advances in Structural Engineering. – 2012. – Vol. 15 (4). – P. 653–664. – DOI: 10.1260/1369-4332.15.4.653.
7. Experimental study on flexural performance of corroded RC beams strengthened with AFRP sheets / Z.-C. Deng, H.-F. Li, L. Wang, L.-P. Zhang // Lin Key Engineering Materials. – 2009. –Vol. 405–406. – P. 343–349. – DOI: 10.4028/www.scientific.net/KEM.405-406.343.
8. CEE 142L reinforced concrete structures laboratory : Beam experiment / Department of Civil and Environmental Engineering. – Los Angeles : University of California, 2002. – URL: https://www.seas.ucla.edu/~wallace/Files%20%20Teaching%20Page/CE%20142L/142L%20beam%20experiment.pdf (date of access: 29.10.2025).
9. Investigation of the shear behavior of concrete beams reinforced with FRP rebars and stirrups using ANN hybridized with genetic algorithm / B. Di, Y. Zheng, R. Qin, J. Lv // Polymers. – 2023. – Vol. 15 (13). – P. 2857. – DOI: 10.3390/polym15132857.
10. Evaluating the ultimate capacity of FRP reinforced concrete beams by using Eurocode 2 and ACI 440.1R-06 / A. Elsheikh, M. Adam, M. Said, A. Salah // Engineering Research Journal (ERJ). – 2024. – Vol. 53 (2). – P. 245–254. – DOI: 10.21608/erjsh.2023.241473.1227.
11. Halahla, A. Study the behavior of reinforced concrete beam using finite element analysis. / A. Halahla // In Proceedings of the 3rd World Congress on Civil, Structural, and Environmental Engineering, April 8–10, 2018, Budapest / Avestia Publishing. – Budapest, 2018. – 9 p. – DOI: 10.11159/icsenm18.103.
12. Karabulut, M. Nonlinear load-deflection analysis of steel rebar-reinforced concrete beams: Experimental, theoretical and machine learning analysis / M. Karabulut // Buildings. – 2025. – Vol. 15 (3). – P. 432. – DOI: 10.3390/buildings15030432.
13. Flexural behavior of concrete beams reinforced with aramid fiber reinforced polymer (AFRP) bars / M. S. Kim, A.-Ch. Kim, Y. H. Lee, A. Scanion // Structural Engineering and Mechanics. – 2011. – Vol. 38 (4). – P. 459–477. – DOI: 10.12989/sem.2011.38.4.459.
14. Li, M. Review on FRP strengthened concrete structures: Current advances, challenges and emerging innovations / M. Li, Y. Du, M. Li // Applied and Computational Engineering. – 2025. – Vol. 172. – P. 18–28. – DOI: 10.54254/2755-2721/2025.GL24467.
15. Renić, T. Ductility of concrete beams reinforced with FRP rebars / T. Renić, T. Kišiček // Buildings. – 2021. – Vol. 11 (9). – P. 424. – DOI: 10.3390/buildings11090424.
16. Saadi, G. M. S. Experimental investigation of CFRP high-strength concrete beams incorporating recycled concrete aggregate / G. M. S.Saadi, M. H. F. Rasheed, A. Z. S. Agha // Buildings. – Vol. 15 (9). – P. 1418. – DOI: 10.3390/buildings15091418.
17. Nonlinear finite element analysis for concrete deep beam reinforced with GFRP bars / M. Said, T. M. El-Rakeeb, A. Salah, N. M. Mohammed // Journal of Engineering Research and Reports. – 2021. – Vol. 21 (12). – P. 43–52. – DOI: 10.9734/jerr/2021/v21i1217517.
18. Sakar, G. Easy prestressing of FRP for strengthening RC beams: Experimental study with an analytical approach / G. H. Sakar, K. Celik // Polymers. – 2025. – Vol. 17 (12). – P. 1628. – DOI: 10.3390/polym17121628.
19. Salem, M. Nonlinear finite element analysis of high and ultra-high strength concrete beams reinforced with FRP bars / M. Salem, M. S. Issa // HBRC Journa. – 2023. – Vol. 19 (1). – P. 15–31. – DOI: 10.1080/16874048.2023.2170765.
20. Sammen, S. S. Nonlinear finite element analysis of concrete beam reinforced with fiber reinforced polymer (FRM) / S. S. Sammen, Q. W. Ahmed, S. N. Al-karawi // IOP Conference Series: Materials Science and Engineering. – Vol. 518 (2). – DOI: 10.1088/1757-899X/518/2/022086.
21. The mechanical and environmental performance of fiber-reinforced polymers in concrete structures: Opportunities, challenges and future directions / S. Sbahieh, U. A. Ebead, S. G. Al-Ghamdi, M. Rabie // Buildings. – 2022. – Vol. 12 (9). – P. 1417. – DOI: 10.3390/buildings12091417.
22. Sbahieh, S. A comparative life cycle assessment of fiber-reinforced polymers as a sustainable reinforcement option in concrete beams / S. Sbahieh, G. McKay, S. G. Al-Ghamdi // Frontiers in Built Environment. – 2023. – Vol. 9. – P. 1194121. – DOI: 10.3389/fbuil.2023.1194121.
23. Experimental study on the flexural performance of GFRP-reinforced concrete beams with a prefabricated permanent UHPC formwork / Y. Su, J. Shang, C. Jin [et al.] // Journal of Composites for Construction. – 2024. – Vol. 29 (1). – DOI: 10.1061/JCCOF2.CCENG-4835.
24. Tran, H. T. Flexural behavior of beams reinforced with FRP bars: Test database, design guideline assessment, and reliability evaluation / H. T. Tran, T. Nguyen-Tho // Buildings. – 2025. – Vol. 15 (18). – P. 3373. – DOI: 10.3390/buildings15183373.
25. Tran, H. N. State-of-the-art review of studies on the flexural behavior and design of FRP-reinforced concrete beams / H. T. Tran, K. C. T. Nguyen, H.-B. Dinh // Materials. – 2025. – Vol. 18 (14). – P. 3295. – DOI: 10.3390/ma18143295.
26. Application of fiber-reinforced polymer (FRP) composites in mitigation measures for dam safety risks: A review / L. Zhao, F. Xiao, P. Lin, G. Bai // Buildings. – 2025. – Vol. 15 (19). – P. 3558. – DOI: 10.3390/buildings15193558.

Material received 08.12.2025, approved 21.12.2025, accepted for publication 22.12.2025